Electronic Supplementary Material (ESI) for RSC Advances.

Supporting information

Modifying Y Zeolite with Chloropropyl for improving Cu load on Y Zeolite as Super Cu/Y Catalyst for Toluene Oxidation

Xiaoling Meng[a], Lingke Meng[a], Yanjun Gong[*a], Zhihong Li[*b], Guang Mo[b], Jing Zhang[b]

a State Key Laboratory of Heavy Oil Processing, The Key Laboratory of Catalysis of CNPC, College of Chemical Engineering, China University of Petroleum (Beijing), 102249, China

b Beijing Synchrotron Radiation Laboratory, Institute of High Energy Physics, Chinese Academy of Sciences, Beijing, China

*Correspondence: gongyj@cup.edu.cn; lzh@ihep.ac.cn;

To determine the optimal amount of CPT addition, the scattering curves of SDA modified by different CPT level (sol-CPT-0.5, 1.0, 1.5 and 2.0) with the aging process are shown in **Fig. S6**. It can be seen that the SAXS curves of sol-CPT-0.5 is similar to sol-con (**Fig. S6a**). The scattering intensity of sol-CPT-0.5 has a tendency to increase with the aging time at low q region (region I) and decreases at high q region (region III). It indicated that the effect of promoting particle growth was not obvious when the CPT additive amount was low. The CPT addition of 1.0 mol.% (sol-CPT-1.0) has been discussed previously, which significantly accelerated the growth of the structure-directing agent. As shown in **Fig. S6c**, continue to increase the content of CPT, the scattering curves of sol-CPT-1.5 is similar to gel.[1] It can be conjectured that CPT in the sol-CPT-1.5 accelerated the growth of the guide agent too fast, resulting in its particle size increased rapidly and beyond the monitoring range of small-angle X-ray scattering detection (1.5-36 nm). With the extension of aging time, there are fewer and fewer particles in the detection range, resulting in a gradual decrease in scattering intensity. The scattering curve of sol-CPT-2.0 has no obvious regularity after the addition of CPT is further increased (**Fig. S6d**). It is assumed that the structure-directing agent under this CPT addition amount has been inactivated.

In order to more intuitively compare the sol scattering curves with different CPT addition amounts, the scattering curves at the same aging time were made on a graph (**Fig. S7**). It can be seen that the intensity of the scattering curves of sol-CPT-1.0 was the highest in the whole aging process. The results showed that sol-CPT-1.0 contains the most active particles and the CPT level (1.0 mol.%) is favorable to accelerate the growth of SDA. The scattering intensity of sol-CPT-0.5 is lower than that of sol-CPT-1.5 and sol-CPT-2.0 at 24 and 48h, but gradually exceeds the latter after 96h. This is because the particles in sol-CPT-0.5 grow gradually and their activity increases

gradually, while too much CPT addition amounts lead to the excessive inactivation of sol-CPT-1.5 and sol-CPT-2.0. Therefore, extra amount or too little CPT addition can not accelerate the growth of the structure-directing agent, and may even cause its inactivation.

The fractal property of the aggregates in sol-CPT-x (x=0.5-2.0) under different aging time are show in **Fig. S8** and **Table S3**. As seen in **Fig. S8**, the fractal dimension of the curves in sol-CPT-0.5 are 1.02 and 1.22 with aging times at 24h and 48 h, respectively. There are little activity when sol-CPT-0.5-24 and sol-CPT-0.5-48 use as SDA. When the aging time prolongated to 96h, the SDA had low activity with the fractal dimension increasing to 1.81. It is worth noting that when the CPT addition amount was 0.5%, the fractal dimension of sol-CPT-0.5 was lower than that of sol-con at the same aging time (**Table S3**). It is indicated that adding a small amount of CPT can not accelerate aging, but retard the growth of particles in SDA. It is speculated that sol-CPT-0.5 hydrolyzed less Si-OH, which was not enough to combine with inorganic substances. Instead, it disrupted the migration of the original aluminosilicate species. Therefore, the sol-CPT-0.5 may take longer (120h) to own high activity. With the increase of CPT addition, the growth rate of particles in the sol-CPT-1.0 significantly improved, as previously described. The fractal dimensions of the sol-CPT-1.0 in all aging times are within the high activity range of the structure-directing agent. Further increase the amount of CPT, the maximum fractal dimensions of the sol-CPT-1.5 under different aging times are 1.51, and it has almost no activity when used as a SDA. It is worth noting that the fractal dimensions of sol-CPT-1.5 decrease after aging at 120h, which indicates that the excessive addition amount of CPT makes the SDA unstable so that it is deactivated quickly. When the amount of CPT further increase, the fractal dimensions of sol-CPT-2.0 are all less

than 1.40. So it can be considered that the sol-CPT-2.0 is in the deactivation state during the whole aging process. In summary, the effect of accelerating the aging of the structure-directing agent is the best when using sol-CPT-1.0 as SDA. Therefore, the addition amount of CPT is selected as 1.0 mol.% in the subsequent experiments.

In order to test the role of the -Cl groups, NaY-CPT zeolite was calcined before Cu-impregnation, the catalyst is denoted as Cu/Y-5-CPT-calcined. Compared with Cu/Y-5-CPT, Cu/Y-5-CPT-calcined exhibits a higher H_2-TPR reduction peak temperature (229 vs 247 °C) (**Fig. S17**). It is speculated that -Cl functional groups was removed from roasting before impregnation, so there was no interaction between -Cl group and Cu, and the metal dispersion was worse than Cu/Y-5-CPT, leading to the reduction ability of Cu/Y-5-CPT-calcined decreased. It is worth noting that the reduction peak above 700°C does not appear in the Cu/Y-5-CPT-calcined, indicating that there is no strong interaction between metal and zeolite support. T_{50} and T_{90} of Cu/Y-5-CPT-calcined were 310 and 356 °C respectively (**Fig. S18**), which were higher than Cu/Y-5-CPT (295 and 335 °C). The role of -Cl group in the preparation of Cu/Y-5-CPT catalyst can be proved.

Supporting Figures and Tables

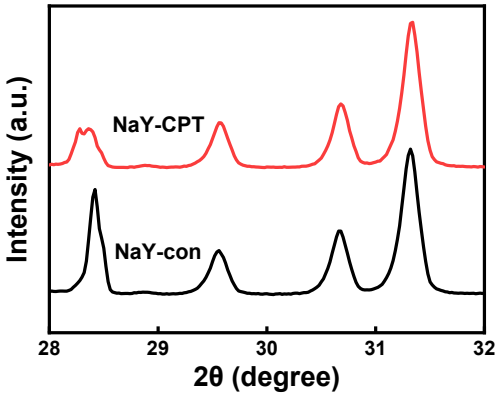

Fig. S1. XRD patterns of NaY-con and NaY-CPT with pure silicon powder as interior label.

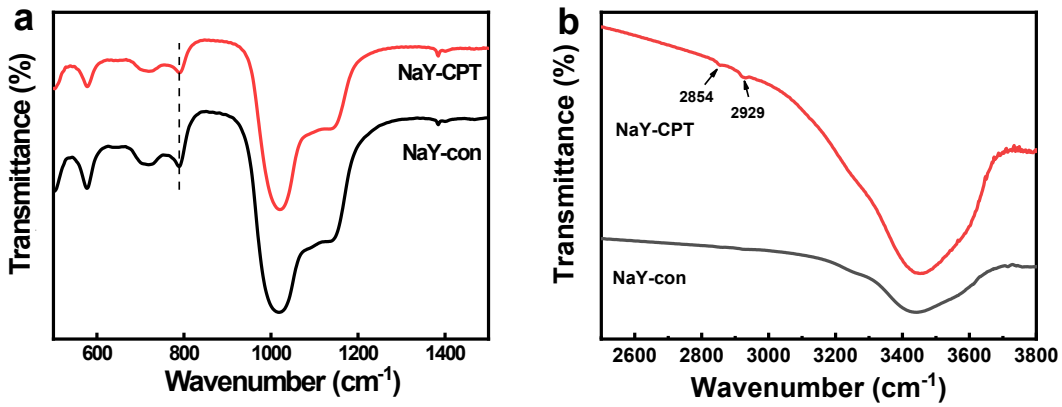

Fig. S2. FT-IR spectra of NaY-con and NaY-CPT.

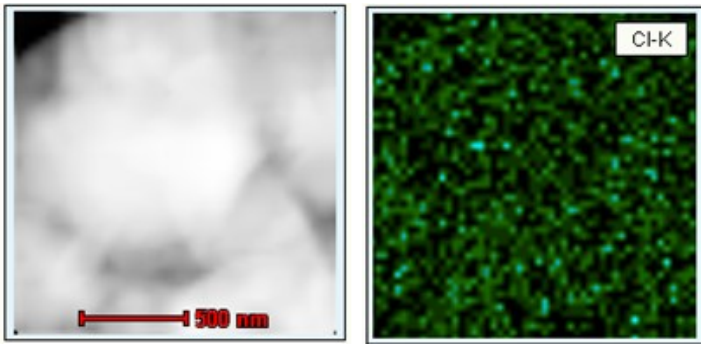

Fig. S3. STEM-EDX elemental mapping image of NaY-CPT.

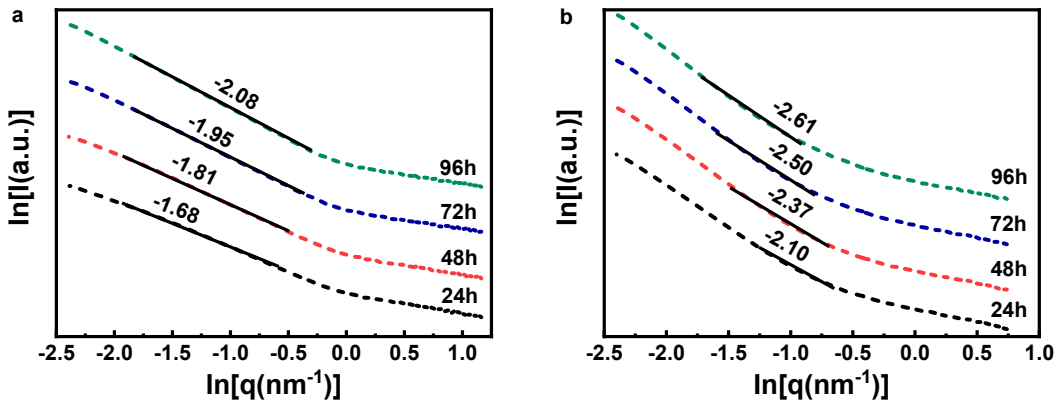

Fig. S4. Fractal dimension of the sol-con (a) and sol-CPT-1.0 (b) sample under different aging time.

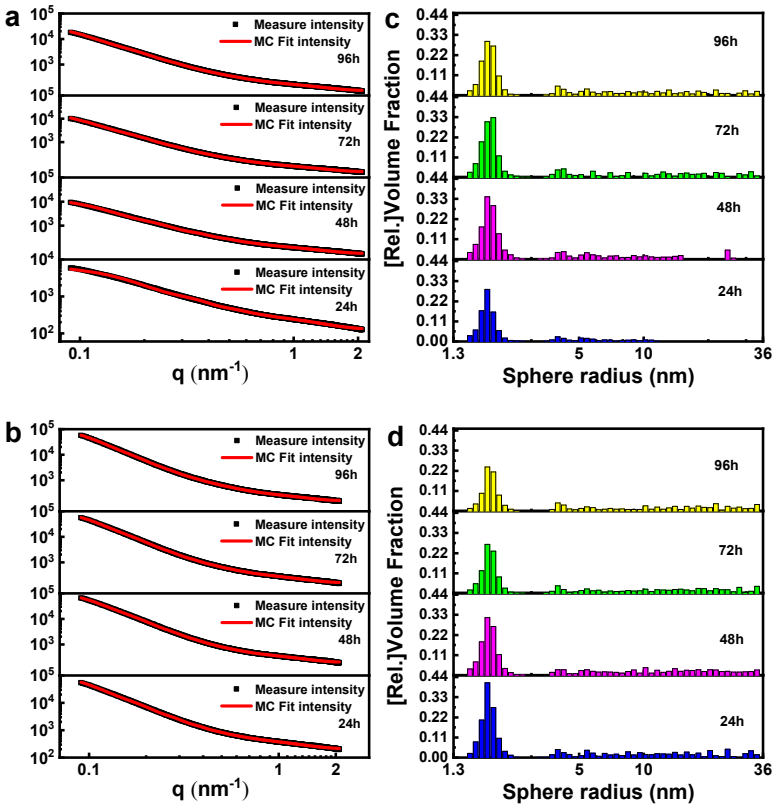

Fig. S5. Monte Carlo fits to the measured SAXS intensity profiles and histograms of the calculated radius size distributions corresponding to the Monte Carlo fits of the sol-con (a,c) and sol-CPT-1.0 (b,d) sample under different aging time.

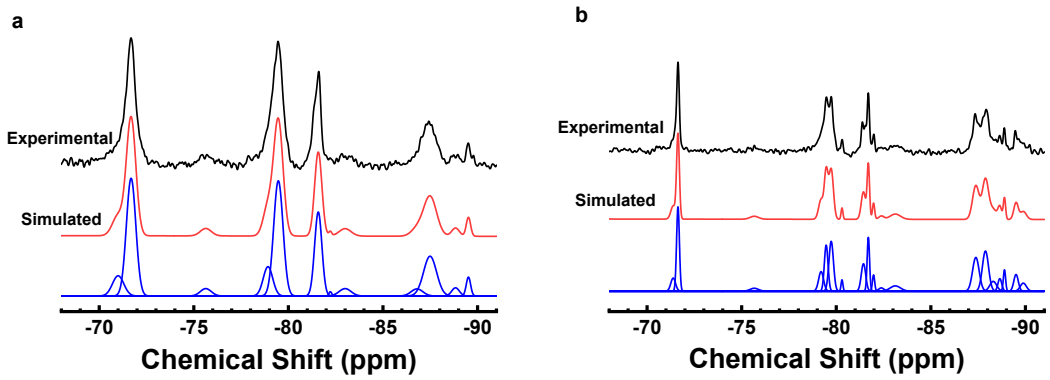

Fig. S6. ^{29}Si NMR spectra of sol-con (a) and sol-CPT-1.0 (b).

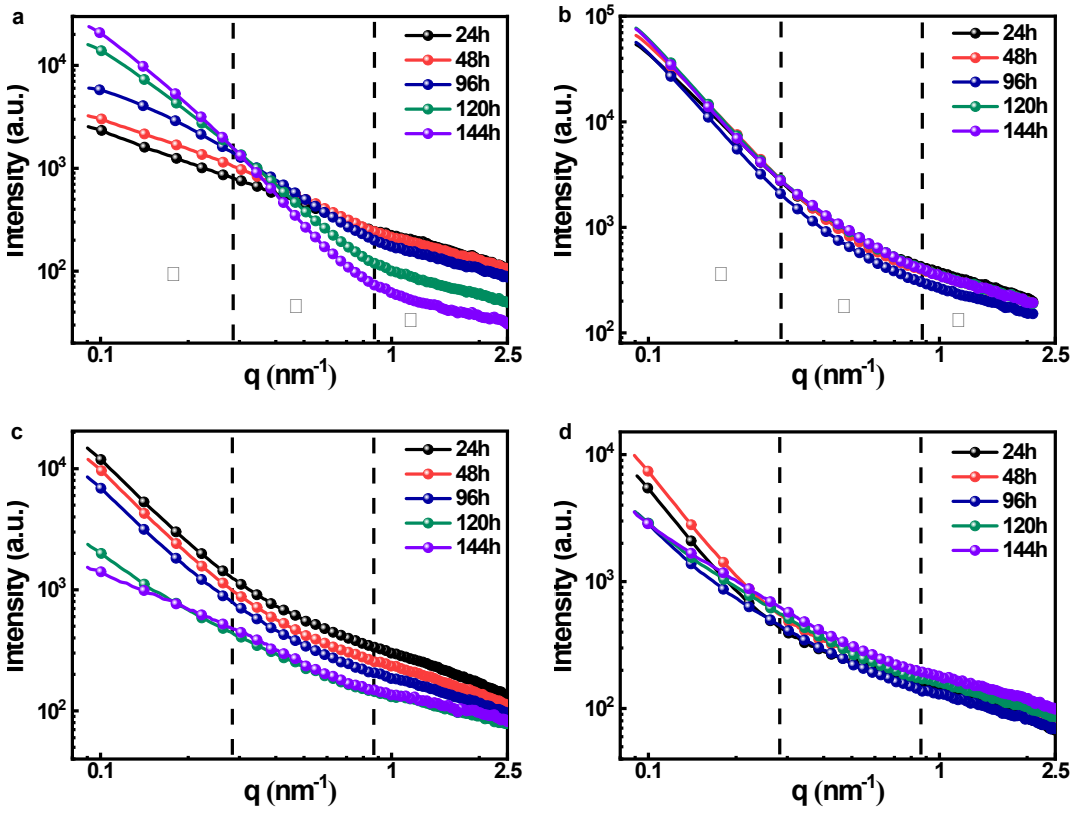

Fig. S7. Scattering curves of the sol-CPT-x samples under different aging time. sol-CPT-0.5 (a), sol-CPT-1.0 (b), sol-CPT-1.5 (c) and sol-CPT-2.0 (d).

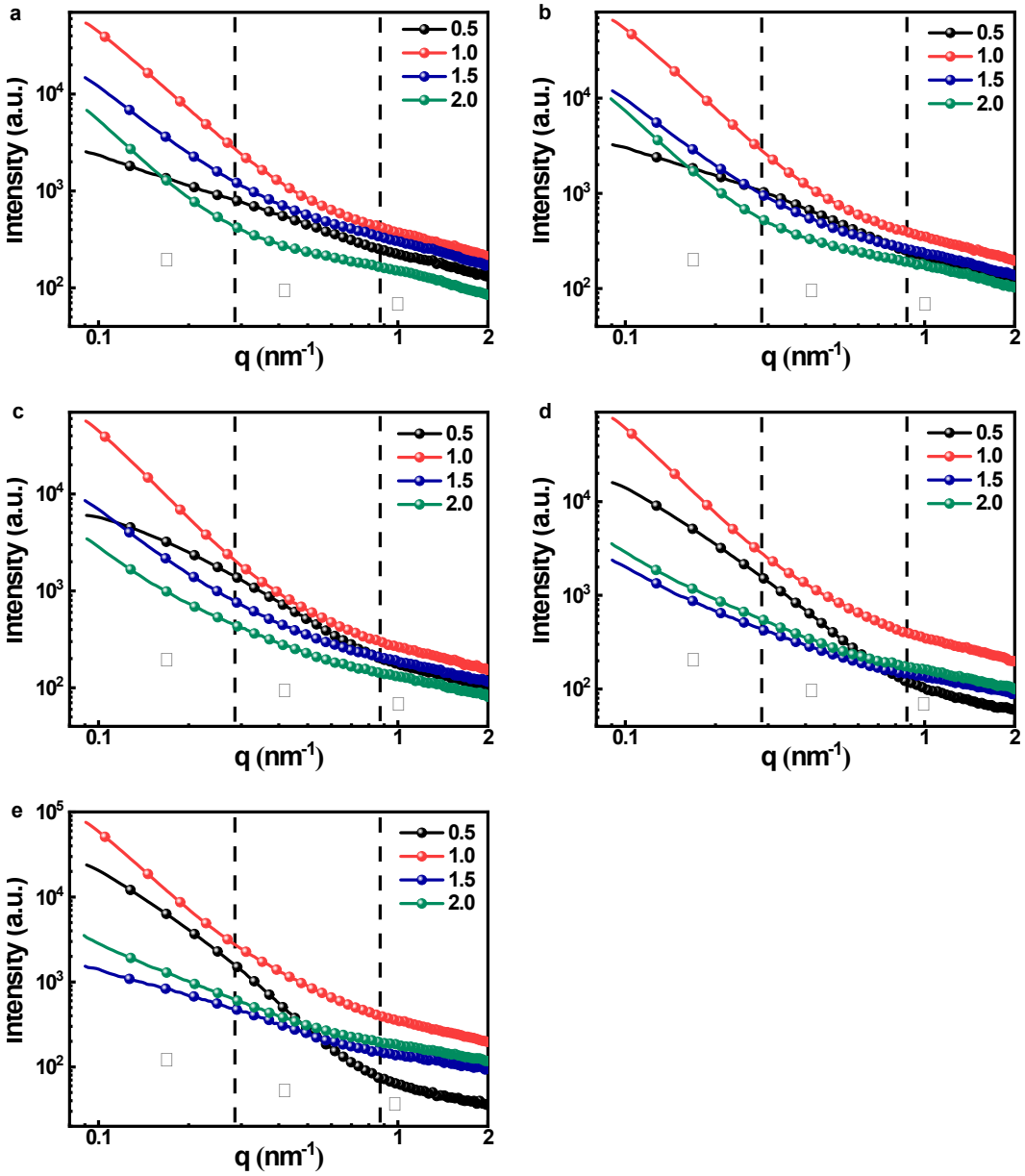

Fig. S8. Scattering curves of the sol-CPT-x (x=0.5-2.0) samples with different CPT level. Aging time: 24h (a), 48h (b), 96h (c), 120h (d) and 144h (e).

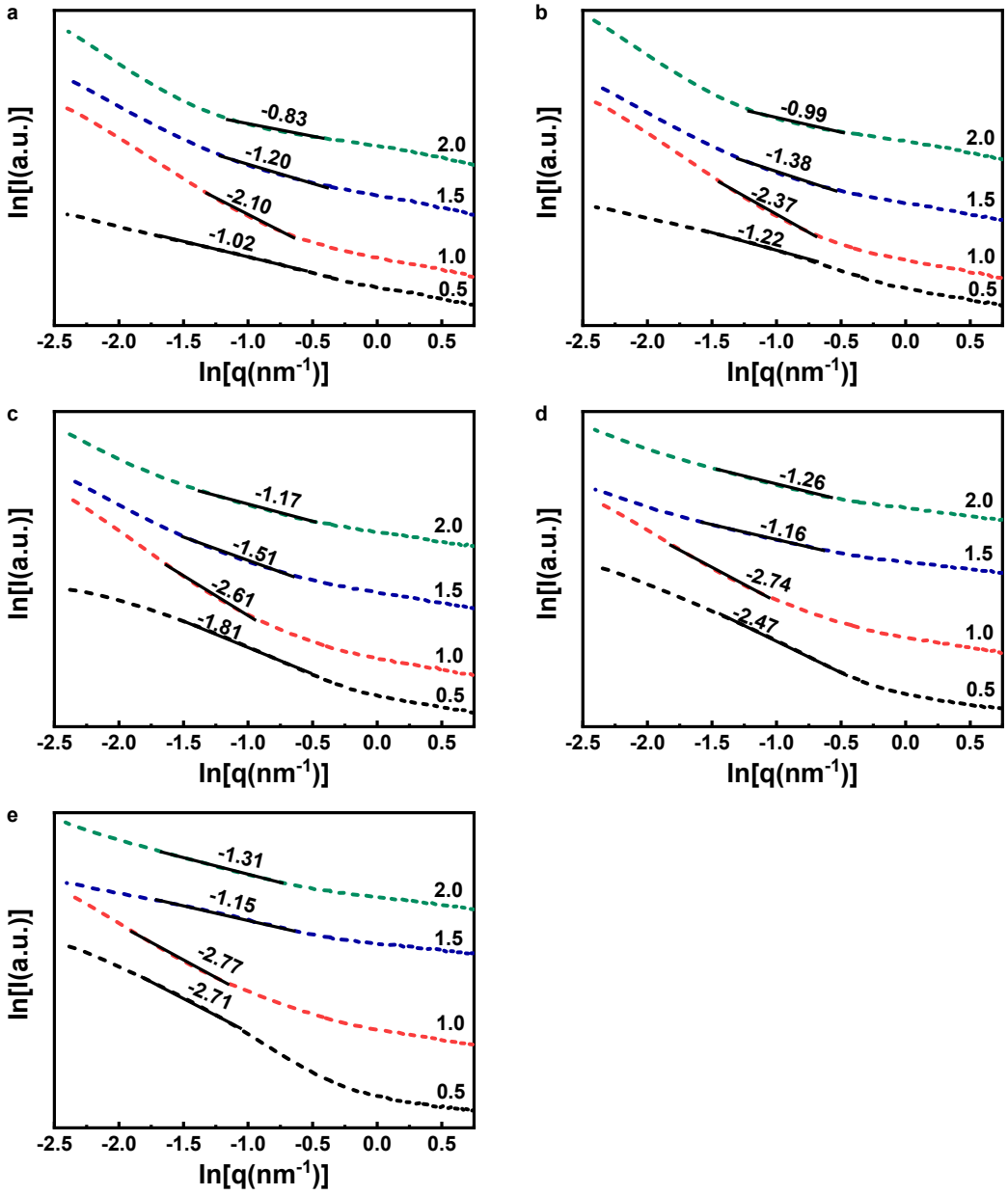

Fig. S9. Fractal dimension of the sol-CPT-x (x=0.5-2.0) samples with different CPT addition amount. Aging time: 24h (a), 48h (b), 96h (c), 120h (d) and 144h (e).

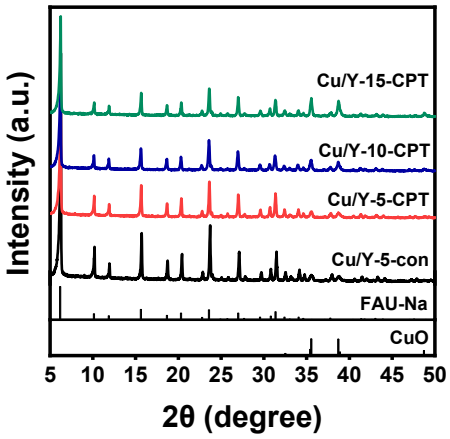

Fig. S10. XRD patterns of Cu/Y-5-con and Cu/Y-x-CPT (x=5-15 wt%).

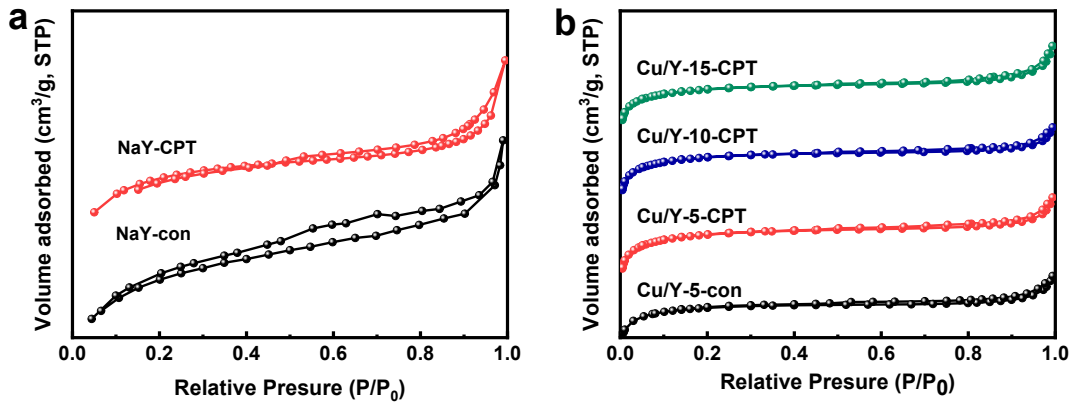

Fig. S11. N_2 adsorption-desorption isotherms of NaY zeolites (a) and Cu/Y catalysts (b).

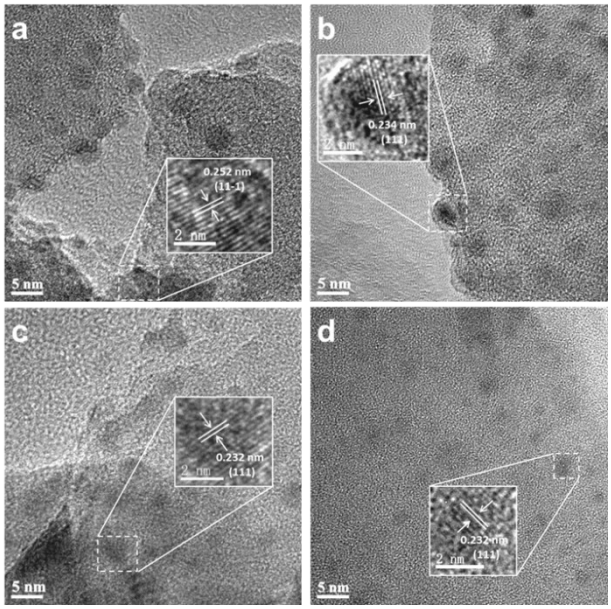

Fig. S12. HRTEM images of Cu/Y-5-con (a), Cu/Y-5-CPT (b), Cu/Y-10-CPT (c) and Cu/Y-15-CPT (d).

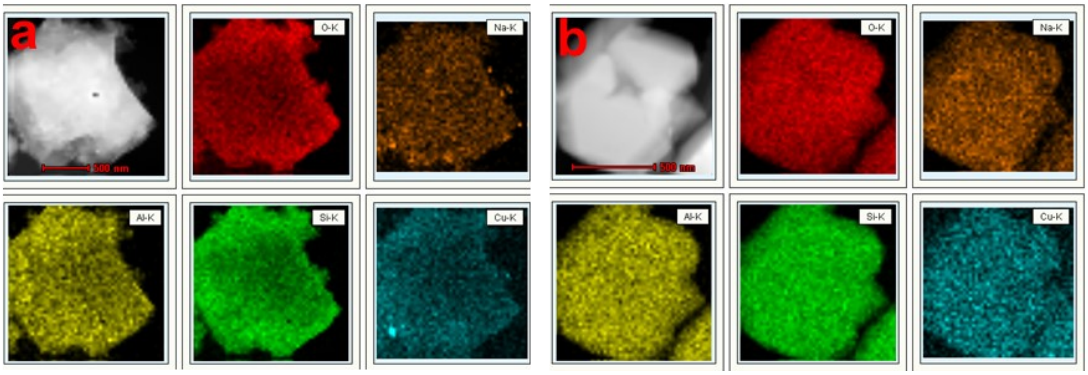

Fig. S13. STEM-EDX elemental mapping image of Cu/Y-5-con (a) and Cu/Y-5-CPT (b).

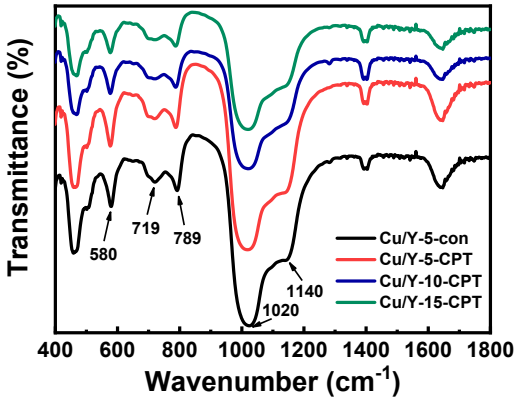

Fig. S14. FT-IR spectra of Cu/Y-5-con and Cu/Y-x-CPT (x=5-15 wt%).

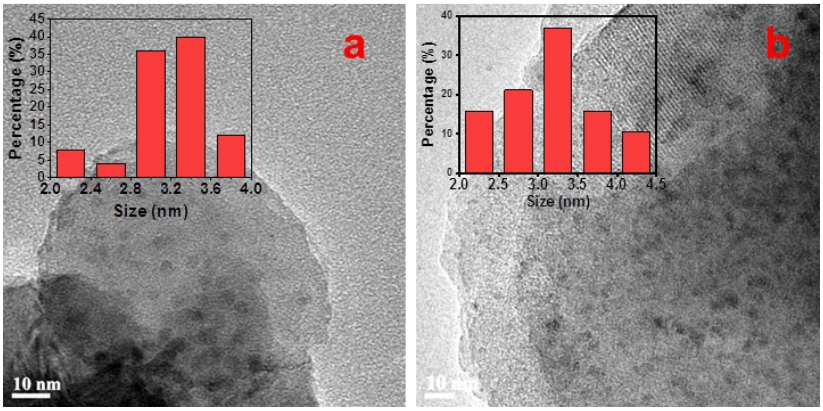

Fig. S15 TEM images of fresh Cu/Y-10-con (a) and used Cu/Y-10-CPT (b).

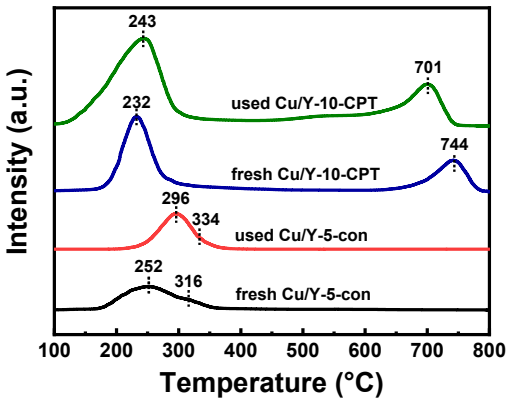

Fig. S16 H_2-TPR profile of fresh and used catalysts.

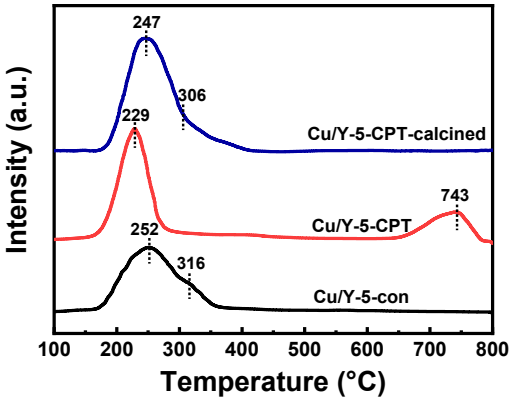

Fig. S17 H_2-TPR profile of Cu/Y-5-con, Cu/Y-5-CPT and Cu/Y-5-CPT-calcined.

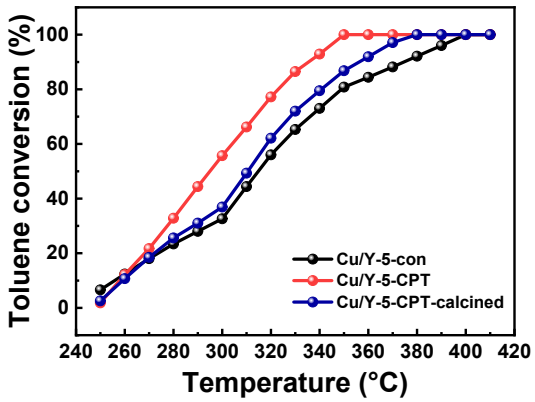

Fig. S18 Toluene catalytic activity of Cu/Y-5-con, Cu/Y-5-CPT and Cu/Y-5-CPT-calcined.

Table S1 Chemical analysis and unit cell value for NaY samples

Samples	CPT/SiO_2	Relative crystallinity/%	SiO_2/Al_2O_3	Peak position/cm^{-1}	N_{Al}
NaY-con	0.00	91	5.35	788.6	49.77
NaY-CPT	0.01	95	6.26	790.7	48.54

Table S2 Peak area of aluminosilicate species in sol derived from ^{29}Si NMR.

Chemical shift (ppm)	Struture	Peak area of sol-con (%)	Peak area of sol-CPT-1.0 (%)
-71.6	monosilicate	30.02	20.52
-75.6	four-membered ring	1.62	0.61
-79.5	dipolysilicate	31.45	26.67
-81.6	three-membered ring	18.27	20.51
-82.2	six-membered ring	0.93	0.69
-83.1	double four-membered ring	1.62	1.11
-87.5	four-membered ring	8.65	17.59
-88.8	double three-membered ring	1.78	7.13
-89.5	double six-membered ring	4.11	5.18

Table S3 Fractal dimension of the sol-x-y with different CPT content and ageing times (x=0.5-2.0, y=24-144h).

Samples	D_m	Activity	Sample	D_m	Activity
sol-0.5-24	1.02	no activity	sol-1.5-24	1.20	no activity
sol-0.5-48	1.22	no activity	sol-1.5-48	1.38	no activity
sol-0.5-96	1.81	low activity	sol-1.5-96	1.51	no activity
sol-0.5-120	2.47	high activity	sol-1.5-120	1.16	no activity
sol-0.5-144	2.71	high activity	sol-1.5-144	1.15	no activity
sol-1.0-24	2.10	high activity	sol-2.0-24	0.83	no activity
sol-1.0-48	2.37	high activity	sol-2.0-48	0.99	no activity
sol-1.0-96	2.61	high activity	sol-2.0-96	1.19	no activity
sol-1.0-120	2.74	high activity	sol-2.0-120	1.26	no activity
sol-1.0-144	2.77	high activity	sol-2.0-144	1.31	no activity

Table S4 Oxidation of toluene over Cu/Y-10-CPT and other catalysts previously reported in the literature

Catalysts	Metal loading (wt.%)	Temp. (°C)	Conv. (%)	Space Velocity (mL g^{-1} h^{-1})	Reference
Cu/Y-10-CPT	10.0	300	98.0	30000	This work
SiBEACo9.0	9.0	320	85.6	60000	[2]
9.5MnO_2/NaCLT	9.5	350	93.0	15000	[3]
Au-Pd/MCM-41	5.6	300	49.0	12000	[4]
Pil-Nb-4.5	4.5	300	56.0	12000	[5]

References:

1. X. Zhao, R. Liu, H. Zhang, Y. Shang, Y. Song, C. Liu, T. Wang, Y. Gong and Z. Li, *Journal of Applied Crystallography*, 2017, **50**, 231-239.
2. A. Rokicinska, M. Drozdek, B. Dudek, B. Gil, P. Michorczyk, D. Brouri, S. Dzwigaj and P. Kustrowski, *Applied Catalysis B-Environmental*, 2017, **212**, 59-67.
3. Z. Ozcelik, G. S. P. Soylu and I. Boz, *Chemical Engineering Journal*, 2009, **155**, 94-100.
4. A. G. M. da Silva, H. V. Fajardo, R. Balzer, L. F. D. Probst, A. S. P. Lovon, J. J. Lovon-Quintana, G. P. Valenca, W. H. Schreine and P. A. Robles-Dutenhefner, *Journal of Power Sources*, 2015, **285**, 460-468.
5. A. J. Schwanke, R. Balzer, C. W. Lopes, D. M. Meira, U. Diaz, A. Corma and S. Pergher, *Chemistry-A European Journal*, 2020, **26**, 10459-10470.